

Effects of spherical confinement and backbone stiffness on flexible polymer jamming

Samuel M. Soik and Tristan A. Sharp

Department of Physics and Astronomy, University of Pennsylvania, Philadelphia, Pennsylvania 19104, USA

(Dated: July 11, 2022)

We use molecular simulations to study jamming of a crumpled bead-spring model polymer in a finite container and compare to jamming of repulsive spheres. Polymer jamming occurs at lower density and with greater variability due to both the container wall and the polymer backbone. In both cases, the onset of rigidity is marked by the creation of a single state of self-stress at isostaticity. However, the confining wall significantly influences internal structure near the wall via density and contact number layering. Combined effects of layering and the backbone bonds are seen in the mechanical response, as reflected by the emergence of additional bands in the vibrational density of states, and in the bulk modulus, which is lower for polymers than monomers and varies with backbone stiffness according to a model of stiffnesses contributing in series.

I. INTRODUCTION

The phenomenon of jamming is observed in systems ranging from granular materials flowing down a chute [1] to DNA packed into a viral capsid [2–4]. Most theoretical understanding of jamming comes from ideal models of granular materials, e.g., simulations of repulsive disks and spheres in periodic boundary conditions (PBC). In general, a packing of a biopolymer into a container involves at least two unavoidable additional features: backbone bonds that link the material into a polymer chain and container walls that change the structure of the material near the boundary. To investigate the consequences of these features, we extend the investigation of jamming to a material with unbreakable adhesive bonds in external spherical confinement (SC).

Jamming occurs as the constituents of a flowing material sufficiently constrain one another’s motion, leading to a configuration that resists applied stress. A central question is whether the material jams *isostatically*, that is, in precise balance of constraints and degrees of freedom, consistent with the boundary conditions. Simulations of frictionless, repulsive disks and spheres in PBC have shown that the onset of rigidity occurs as a jump in particle-particle coordination number from zero to twice the dimensionality: four for disks and six for spheres, which corresponds to isostaticity [5–12]. We show that jamming in our simulations, with backbone bonds and a concave confining wall, occurs isostatically in the same way as for repulsive spheres.

Repulsive spheres typically jam at a packing fraction of about 64%, which corresponds to the density of the maximally-random jammed (MRJ) state [5, 6, 13–18]. Unlike repulsive spheres, a bead-spring model polymer has “built-in” constraints provided by backbone bonds. Isostatic packings of flexible chains can be obtained at ϕ^{MRJ} using algorithms that eliminate the effects of connectivity and allow effective equilibration through entanglements and knotting [19–27]. However, with more realistic dynamics, chains jam at about 2% below ϕ^{MRJ} in PBC with little system-size dependence and retain a significant fraction of unconstrained degrees of freedom [28]. Confinement also reduces the jamming density by

inducing layering near the boundary [29–39]. We present both the reduction in density due to SC alone using repulsive sphere packings and further reduction due to the polymer backbone.

On the other hand, few studies of polymer packings in confined geometries address mechanical properties. Previous investigations have largely focused on chain conformation within the packing [40–44] and topological ordering of segments [45]. Long polymers with specified bond-bond angles typically coil during packaging in SC to minimize bending energy [46–52] and thus exhibit boundary-induced layering [50]. In contrast, we use a crumpled, flexible-chain model to avoid coiling [49] and to focus on the role of backbone connectivity in distinguishing the polymer from the monomer systems.

We first explain the constraint-counting that causes jamming in the presence of external confinement and adhesive bonds (Sec. III). We present the theory underlying our results and explain how, due to unique considerations of systems in external confinement, coordination number becomes less appropriate in assessing the onset of rigidity. In Sec. IV A, we show that the same understanding of states of self-stress and zero modes in repulsive sphere packings extends to the case of a polymer in SC. In Sec. IV B, we provide the distribution of jamming densities in simulations of spherically-confined polymers and compare to those of monomers in SC and in PBC to isolate the effects of backbone bonds and the confining wall. We find boundary-induced order in local density and coordination (Sec. IV C) and in the vibrational density of states, with effects on band structure due to the confining wall, pressure, and the backbone (Sec. IV D). Finally, we discuss the effects of structural differences on the bulk modulus in comparing monomers to polymers as well as polymers with varying backbone stiffness (Sec. IV E).

II. SIMULATION DETAILS

To study jamming of flexible polymers, we use 3D molecular dynamics simulations [53] with $256 \leq N \leq 8192$ monodisperse, frictionless, spherical particles of diameter σ . Each particle represents a monomer along a

polymer chain, and interactions are governed by the following potentials:

$$V_0(r_{ij}) = \frac{\varepsilon_0}{2} \left(1 - \frac{r_{ij}}{\sigma}\right)^2 \theta\left(1 - \frac{r_{ij}}{\sigma}\right) \quad (1a)$$

$$V_B(r_{kl}) = \frac{\varepsilon_B}{2} \left(1 - \frac{r_{kl}}{\sigma}\right)^2 \quad (1b)$$

$$V_W(r_i) = \frac{\varepsilon_W}{2} \left(\frac{1}{2} - \frac{R - r_i}{\sigma}\right)^2 \theta\left(\frac{1}{2} - \frac{R - r_i}{\sigma}\right). \quad (1c)$$

Nonconsecutive monomers interact via the harmonic repulsive potential $V_0(r_{ij})$, where r_{ij} is the distance between the centers of particles (also referred to as *sites*) i and j , ε_0 is the characteristic energy, and $\theta(x)$ is the Heaviside step function. Consecutive monomers k and l are bound by the two-sided harmonic potential $V_B(r_{kl})$, so that backbone bonds have energy scale ε_B and rest length σ . To induce jamming, the polymer is confined by a spherical wall centered at the origin according to the radial harmonic potential $V_W(r_i)$, where r_i is the radial coordinate of site i and R is the wall radius. The total potential energy \mathcal{E} is the sum of all pairwise and wall potentials. We consider at each site an equal point mass m , which sets the mass scale, and energies will be reported in units of ε_0 , distances in units of σ , pressures in units of ε_0/σ^3 , and frequencies in units of $\sqrt{\varepsilon_0/m\sigma^2}$.

Disordered configurations are generated by thermalizing the polymer chains at temperature $kT = 0.003$ in a large confining sphere at packing fraction $\phi = N \left(\frac{\sigma}{2R}\right)^3 = 0.02$. Each thermal configuration is then quenched to $T = 0$ using the FIRE algorithm [54]. We compress each quenched system in small increments $\Delta\phi \leq 0.01$ by decreasing R and minimizing energy after each compression until a jammed configuration is obtained, indicated by a nonzero \mathcal{E} . We then expand or compress these configurations to within 1% of each target pressure $p \equiv -\partial\mathcal{E}/\partial V$, where the system volume $V = 4\pi R^3/3$ is that bounded by the confining sphere. For each system of size N , at least 100 random configurations are prepared, and each of these is studied at a large range of target pressures $10^{-7} \leq p \leq 10^{-1}$, bond energies $0.1 \leq \varepsilon_B \leq 10$, and wall energies $0.1 \leq \varepsilon_W \leq 10$.

The same procedures are repeated for unbonded monomers in SC (where $\varepsilon_B = 0$) and in PBC [where $\varepsilon_W = \varepsilon_B = 0$ and $\phi = \frac{\pi N}{6} \left(\frac{\sigma}{2R}\right)^3$ in a cubic domain with side length $2R$].

III. ISOSTATICITY AND COORDINATION

We review the analysis of the mechanical constraints that resist deformations and cause jamming. This allows us to introduce the effects of confining walls and adhesive bonds. Starting from a static configuration after energy minimization, i.e., in force balance, we consider the Taylor-expansion of the energy in terms of displacements. As shown explicitly in the Appendix, the terms of quadratic order in displacements contain, in addition

to displacements parallel to the interaction direction, displacements perpendicular to the interaction direction. If \mathbf{r}_{ij} is the relative position of particles i and j , where $r_{ij} = |\mathbf{r}_{ij}|$, then consider the change in energy from an interaction potential due to a small displacement that is perpendicular to \mathbf{r}_{ij} , \mathbf{r}_{kl} , or \mathbf{r}_i [cf. Eq. (1)]. These are

$$\Delta V_0(u_\perp) = \frac{\varepsilon_0}{2} \left(1 - \frac{\sigma}{r_{ij}}\right) \left(\frac{u_\perp}{\sigma}\right)^2 + O(u_\perp^4) \quad (2a)$$

$$\Delta V_B(u_\perp) = \frac{\varepsilon_B}{2} \left(1 - \frac{\sigma}{r_{kl}}\right) \left(\frac{u_\perp}{\sigma}\right)^2 + O(u_\perp^4) \quad (2b)$$

$$\Delta V_W(u_\perp) = \frac{\varepsilon_W}{2} \left(1 - \frac{R - \sigma/2}{r_i}\right) \left(\frac{u_\perp}{\sigma}\right)^2 + O(u_\perp^4), \quad (2c)$$

where u_\perp is the magnitude of the perpendicular displacement, and we have omitted the Heaviside function $\theta(x)$ for brevity. The prefactor of the quadratic term is negative for overlapping monomers, so energy decreases in the perpendicular direction, and the particles tend to slip off one another. In contrast, small displacements perpendicular to extended backbone bonds ($r_{kl} > \sigma$) or tangential to the wall instead require an increase in energy; these result in linear restoring forces perpendicular to the interaction. The prefactors vanish in the unstressed, i.e., zero-energy limit, so the energy costs of perpendicular motions appear only at $O(u_\perp^4)$, and have no linear response.

When interested in the linear response at low pressure, near jamming, we often consider the unstressed network of a given system by replacing all contacts (including backbone bonds and wall contacts) with unstretched harmonic springs in an analysis following Ref. [55]. The mapping to the spring system is exact in the limit of zero pressure, and each spring introduces one harmonic constraint.

Each contact $i' \leq N_C$, where N_C is the number of contacts, is replaced by a harmonic bond of rest length $r_{i'}$ equal to r_{ij} , r_{kl} , or $R - r_i$ [referring to Eq. (1)] depending on the interaction. In the following, we use Einstein notation, and sites are labeled by plain Roman indices, bonds by primed Roman indices, and Cartesian components by Greek indices. Site displacements form the dN -dimensional displacement vector U_i^μ , where μ indexes the $d = 3$ Cartesian components of each vector \mathbf{u}_i . The linear operator $C_{i'\mu}^i$, termed the compatibility matrix, maps U_i^μ to the N_C -dimensional bond elongation vector $E_{i'} \equiv \frac{\partial r_{i'}}{\partial r_i^\mu} U_i^\mu$:

$$C_{i'\mu}^i U_i^\mu = E_{i'}. \quad (3)$$

Since a zero mode is described by a set of displacements that causes no bond elongations, the nullspace of $C_{i'\mu}^i$ is spanned by modes associated with both floppy modes and global rigid-body motions, of which there are in total

$$N_0 = \text{nullity}(C_{i'\mu}^i). \quad (4)$$

Conversely, we may consider the resulting force on each site as the linear response to a tension vector, $F_i^\mu \equiv -\frac{\partial r_i^{\nu'}}{\partial r_i^\mu} T_{i\nu}'$. We then obtain the equilibrium matrix:

$$Q_i^{i'\mu} T_{i'\nu}' = -F_i^\mu. \quad (5)$$

Comparing with Eq. (3), we see that, in matrix form, $Q_i^{i'\mu}$ is the transpose of $C_{i'\mu}^i$.

In certain networks, the bonds may be placed under tension or compression while maintaining zero net force on each site, i.e., $Q_i^{i'\mu} T_{i'\nu}' = 0$. Such a tensional state $T_{i'\nu}'^S$ is referred to as a state of self-stress (SSS) and is contained in the nullspace of $Q_i^{i'\mu}$. The number of SSSs in a system is thus given by

$$N_S = \text{nullity}(Q_i^{i'\mu}) = \text{nullity}(C_{i'\mu}^i). \quad (6)$$

From the rank-nullity theorem, and given $\text{rank}(C_{i'\mu}^i) = \text{rank}(Q_i^{i'\mu})$, we obtain the Index theorem [55]:

$$N_0 - N_S = dN - N_C. \quad (7)$$

Creating a rigid d -dimensional packing of spheres requires the number of constraints to match or exceed the degrees of freedom to be constrained [56], i.e., $N_C \geq dN - f(d)$, where $f(d)$ is the number of zero modes associated with rigid-body motions. PBC permit $f(d) = d$ rigid translations while a frictionless, $(d-1)$ -spherical boundary permits $f(d) = \frac{1}{2}d(d-1)$ rigid rotations. By its strictest definition [55], an isostatic system contains neither floppy modes nor SSSs [$N_0 = f(d)$, $N_S = 0$]; however, jammed packings necessarily have at least one SSS ($N_S \geq 1$) corresponding to a non-zero modulus [6, 8], so that the number of contacts of a jammed isostatic system is $N_C^{\text{iso}} = dN - f(d) + 1$. Each additional constraint added to such a system creates an additional SSS:

$$N_S = N_C - N_C^{\text{iso}} + 1. \quad (8)$$

Constraints in repulsive sphere packings are commonly characterized by the coordination number

$$z = \frac{1}{N} \sum_{i=1}^N z_i, \quad (9)$$

where z_i is the number of contacts of particle i , but this is less appropriate in confinement. First, without external confinement, as in PBC, all contacts are between two particles, so $z = \frac{2N_C}{N}$ is twice the contact density, and the relation between N_S and z is

$$\frac{N_S}{N} = \frac{\Delta z}{2} \equiv \frac{z - z^{\text{iso}}}{2} \quad (10)$$

with $z^{\text{iso}} = \frac{2N_C^{\text{iso}}}{N} = 2d - \frac{2f(d)}{N}$. However, in external confinement, each wall contact involves only one particle. Since the wall itself is not counted as a particle, wall contacts do not get double-counted, and the coordination

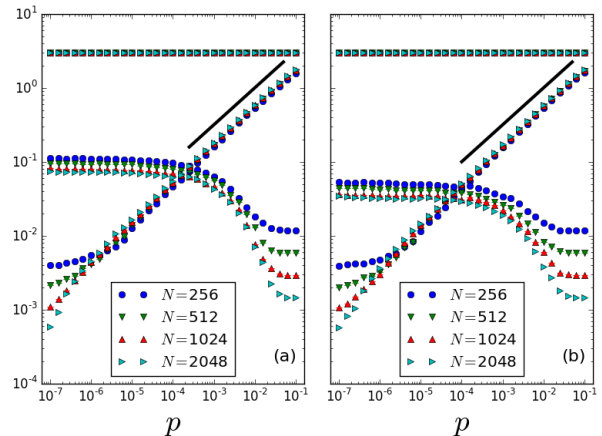


FIG. 1. Selected Index theorem values for (a) monomers ($\varepsilon_W = 1$) and (b) polymers ($\varepsilon_B = \varepsilon_W = 1$). Monotonically increasing (decreasing) curves show N_S/N (N_0/N). Upper curves show computational results for $(N_C + N_0 - N_S)/N$, equal to the dimensionality $d = 3$ as guaranteed by Eq. (7). Black lines have slope $1/2$. Approximately 100 states of each system size and pressure are considered.

number z is lower than twice the contact density by an amount that decreases with system size:

$$\frac{2N_C}{N} - z = \frac{N_W}{N} \sim \frac{1}{L}, \quad (11)$$

where N_W is the number of wall contacts, and $L \equiv N^{1/d}$ is the linear system size. Therefore, z is twice the density of constraints only when each contact constrains two degrees of freedom.

Second, previous studies of monomers have removed rattlers in order to isolate the rigid subsystem for a clear computation of Δz [6, 8]. Due to unbreakable bonds, polymers instead contain particles called flippers, which are only constrained by backbone bonds and thus can freely move tangent to their neighbors. To accurately analyze the rigid subsystem of a confined polymer, a direct computation of Δz requires both a boundary correction and the removal of all flippers and the backbone bonds constraining them.

IV. RESULTS

A. States of self-stress and zero modes

In Fig. 1, we compute N_S . Our results show that $N_S \geq 1$ as seen in the splitting of N_S/N curves to $1/N$ in the low- p limit. Jamming in our systems, even with adhesive bonds and confinement, therefore corresponds to the introduction of a single SSS. For the polymers, the SSS may contain both extended and compressed backbone bonds; indeed we find that $\approx 30\%$ of backbone bonds are extended near the jamming transition, so the ratio of extended to compressed backbone bonds is ≈ 0.5 .

We see the power-scaling law $N_S/N \sim \Delta z \sim p^{1/2}$, the same as for spheres [6, 8], for both monomers and polymers ($\varepsilon_B = 1$) in confinement. This may be contrasted with a perfect d -dimensional crystal in external confinement, which would contain $N_S \gtrsim L^{d-1}$ at $p \rightarrow 0^+$. The increasing number of SSS involve an increasing number of sites (N_C^{rigid}) and engaged contacts (N_C^{rigid}) as the rigid subsystem grows.

To quantify the number of unconstrained motions, we compute N_0 . We find that $N_0^{\text{mono}} > N_0^{\text{poly}}$ in the low- p limit. For monomers, these are primarily rattlers, which have no constraints, so each contributes $d = 3$ zero modes. For polymers, these are primarily flippers; the smaller number of zero modes reflects the extra constraints from the backbone bonds that constrain motion even on particles outside the rigid subsystem. The two particles at the ends of the chain are called *terminal* sites while all other particles within the chain are called *internal*. Terminal (internal) sites in polymer systems have at least 1 (2) constraint(s) due to backbone bonds; as such, terminal filaments contribute $(d - 1)N_f$ zero modes, and internal filaments contribute $(d - 1)N_f - 1$ zero modes. (In the exceptionally rare case of two collinear, unstressed bonds around an internal site, only one constraint would be introduced, with two zero modes retained.) Here, *filament* refers to a group of N_f consecutive flippers on a polymer; a filament is considered terminal if it contains a terminal site. Directly computing the precise number of flippers requires distinguishing the topologically-distinct filament types and is not necessary to see that about 1–2% of the degrees of freedom are unconstrained even at moderate pressures. The significant number of unconstrained motions is consistent with other realistic packing protocols [57, 58].

The fraction of rattlers (flippers) decreases with system size. In the high- p limit, no rattlers (flippers) remain, as all particles become sufficiently coordinated that the only remaining zero modes are those associated with $f(d)$ rigid rotations within the spherical container.

Next, we delete the rattlers and flippers, isolating the N^{rigid} particles and N_C^{rigid} engaged contacts of the rigid subsystem. At all pressures, we find that the number of zero modes that remain is again $f(d)$, indicating that no other zero modes are present in the rigid subsystem. Therefore, from Eq. (7),

$$\lim_{p \rightarrow 0^+} N_C^{\text{rigid}} = dN^{\text{rigid}} - f(d) + 1 = N_C^{\text{rigid,iso}}, \quad (12)$$

and we find that the rigid subsystem jams isostatically.

B. Packing fraction at jamming

Fig. 2 shows the fraction of systems that are jammed f_J at packing fraction ϕ as well as the average packing fraction at jamming ϕ_J^N for $256 \leq N \leq 8192$. Monomers in PBC jam near 64%, as expected for MRJ states, for all system sizes. Confinement shifts jamming distributions

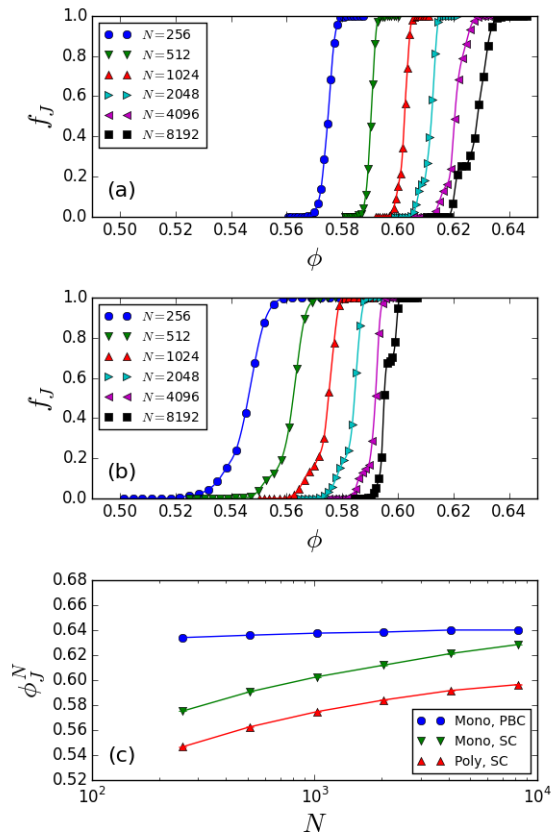


FIG. 2. Fraction of jammed states for (a) monomers and (b) polymers ($\varepsilon_B = 1$) in SC ($\varepsilon_W = 1$). (c) Comparison of $\phi_J^{N,\text{mono}}$ and $\phi_J^{N,\text{poly}}$ in SC to monomers in PBC. Approximately 500 states (250 for the largest systems) of each system size are considered.

to lower densities and increases system-size dependence. $\phi_J^{N,\text{mono}} < \phi^{\text{MRJ}}$ [Fig. 2(a, c)], in agreement with previous studies of confined monomers [29, 30, 36, 37]. The deviation of ϕ_J from ϕ^{MRJ} is almost 6% at $N = 256$ and diminishes to less than 1% by $N = 8192$.

The inclusion of unbreakable backbone bonds further reduces the jamming density to almost 10% below ϕ^{MRJ} at $N = 256$, and remains more than 4% lower at $N = 8192$. We see that $\phi_J^{N,\text{mono}} > \phi_J^{N,\text{poly}}$ in SC, due to the constraints arising from the polymer backbone. Backbone bonds prevent consecutive polymer sites from drifting apart during the approach to jamming and also lead to attractive forces in extension. Constraining effects of the backbone do not strongly diminish with system size; the $\approx 4\%$ difference between $\phi_J^{N,\text{mono}}$ and $\phi_J^{N,\text{poly}}$ persists across system sizes, similar to the density shift seen in jamming of flexible, thermal polymers in PBC [28]. Backbone bond stiffness has no appreciable effect on $\phi_J^{N,\text{poly}}$ of flexible polymers, so only $\varepsilon_B = 1$ data are shown in Fig. 2.

Finally, the width of the jamming distribution substantially widens with decreasing system size, especially for

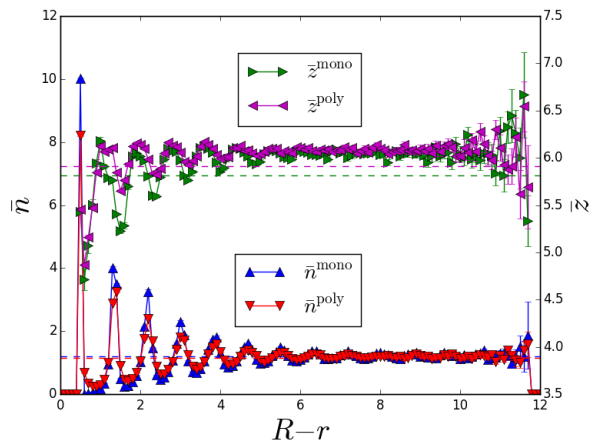


FIG. 3. Average local number density \bar{n} (lower curves, left axis) and average local coordination \bar{z} (upper curves, right axis) for $N = 8192$ systems ($\varepsilon_W = \varepsilon_B = 1$) at $p = 10^{-4}$. Dashed horizontal lines are the global number density n and coordination number z for the system. Curves are averages of approximately 100 configurations.

polymers.

C. Boundary-induced structure

We compute the average local number density \bar{n} and average local coordination \bar{z} by binning point masses at $\{\mathbf{r}_i\}$ and their respective coordination values $\{z_i\}$ over distance from the boundary $R-r$ (Fig. 3). Density layering is significant near the boundary (and, as reflected in Fig. 1, reduces ϕ_J^N). The global number density n and coordination number z are shown as dashed lines in Fig. 3. Oscillations occur in both \bar{n} and \bar{z} , similar to previous density profiles of confined monomers determined in experiments [30, 31] and simulations [32–37, 50]. Both oscillatory periods are consistent with the height of a regular tetrahedron (3-simplex), $\sqrt{2/3}\sigma \approx 0.82\sigma$, and agree with the well-established polytetrahedral structure of jammed monomer [59, 60] and polymer [23–27] states. We note that sharply-peaked maxima (minima) in \bar{n} (\bar{z}) are separated by broad, rounded minima (maxima). This qualitative “inversion” of curves would suggest that sites of high-density layers are, perhaps unintuitively, *less* coordinated than sites in the low-density layers between them. This could be rationalized by considering that particles in high-density layers sit between two lower-density layers, with which they have fewer contacts than particles in low-density layers that sit between two high-density layers. However, the structure is even more complex than this, as \bar{z} curves are also shifted to the right of their inverted \bar{n} counterparts; qualitatively, this phase shift appears to be about one-quarter of the period.

While the curves are similar for monomers and polymers, a first noticeable difference is the height of the initial

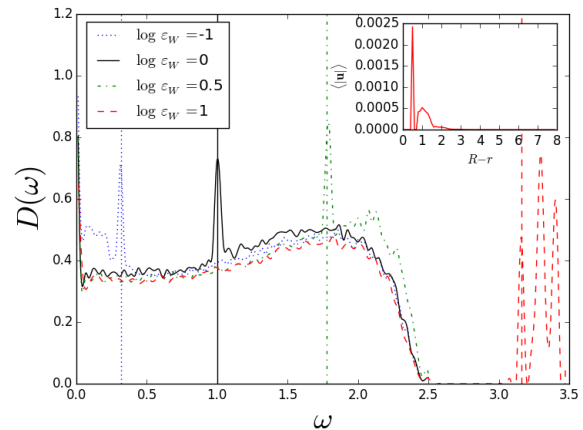


FIG. 4. $D(\omega)$ at $p = 10^{-4}$ and $0.1 \leq \varepsilon_W \leq 10$ for a $N = 2048$ monomer system. Vertical lines indicate corresponding ω_W values. Inset: average displacement for eigenstates $\{U_i^\mu : \omega > 3, \varepsilon_W = 10\}$.

narrow peak at $R-r = \sigma/2$, indicating $N_W^{\text{mono}} > N_W^{\text{poly}}$, which becomes important to the bulk modulus as considered in Sec. IVE 1. Additionally, for polymers, the oscillation amplitude of \bar{n} is noticeably less than that of monomers, indicating that polymers exhibit less-extreme layering. In contrast, $\bar{z}^{\text{mono}} < \bar{z}^{\text{poly}}$ at nearly all points because of backbone bonds retained by flippers, which lead to the higher global coordination z of polymers than monomer systems with fully-uncoordinated rattlers.

D. Density of states

To investigate the vibrational density of states, we construct the $dN \times dN$ dynamical matrix

$$D_{i\nu}^{j\mu} = \frac{1}{m} C_i^{i'\mu} K_{i'}^{j'\nu} C_{j'\nu}^j = \frac{1}{m} Q_i^{i'\mu} K_{i'}^{j'\nu} Q_{j'\nu}^j, \quad (13)$$

where $K_{i'}^{j'\nu} \equiv \partial^2 V(r_{i'}) / \partial r_{j'}^2$ is the diagonal stiffness matrix. The set of eigenvectors $\{U_i^\mu\}$ of $D_{i\nu}^{j\mu}$ are the polarization vectors of the system’s normal modes, and the eigenvalues $\{\lambda\} = \{\omega^2\}$ are the squared frequencies of the normal modes [61]. From $\{\omega\}$, we compute the density of states $D(\omega)$. Since there is little variation among system sizes, we present only $N = 2048$ data.

1. Boundary modes

We compute the density of states $D(\omega)$ in systems with wall potentials $0.1 \leq \varepsilon_W \leq 10$ for monomers in SC (Fig. 4). We first note that peaks at $\omega = 0$ represent zero modes due to rattlers and rigid rotations. The curves have the universal characteristic shape seen previously in disordered systems in PBC [6], the so-called

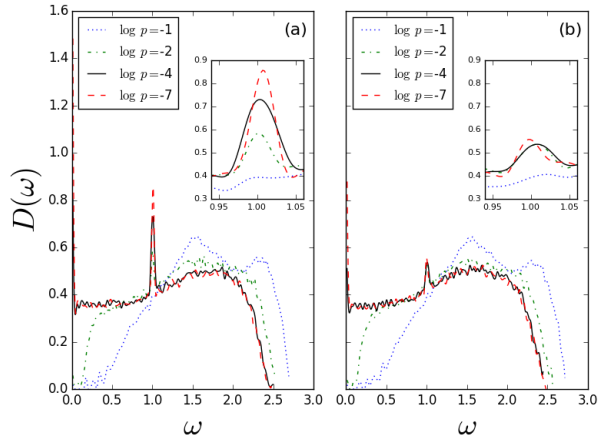


FIG. 5. $D(\omega)$ ($\varepsilon_W = 1$) for (a) $N = 2048$ monomer and (b) $N = 2048$ polymer ($\varepsilon_B = 1$) systems. Insets show zoomed-in view of boundary-mode peaks.

boson peak at small finite ω . However, wall potentials induce N_W boundary modes with typical frequencies of $\omega_W \equiv \sqrt{\varepsilon_W/m\sigma^2}$, resulting in additional pronounced peaks.

At large ε_W , the additional modes lead to a band gap in $D(\omega)$. In this case, modes with $\omega > 3$ may be isolated, and we bin the total set of polarization magnitudes $\{|\mathbf{u}_i|\}$ over $R-r$ to compute the average polarization $\langle|\mathbf{u}|\rangle$ with respect to distance from the wall (Fig. 4 inset). The boundary modes are almost entirely localized to the two layers of sites nearest the boundary, giving the two distinct peaks in $\langle|\mathbf{u}|\rangle$.

2. Pressure effect

Having accounted for the origin of the peak at ω_W , we compare $D(\omega)$ at varying pressure in Fig. 5. In agreement with Fig. 1, the zero-mode peak is taller at lower p and generally taller for monomers than polymers at the same p . The boundary-mode peak associated with ε_W is consistent across system types for $p \leq 10^{-2}$. We note that this peak becomes shorter at higher p in monomer systems [see Fig. 5(a) inset], despite an increase in N_W which necessarily arises at higher p . Instead, the decrease in height indicates that the distribution of boundary-mode frequencies, which is narrow at low p , broadens with increasing p until the peak is seen to converge with the bulk band at $p = 10^{-1}$. However, the analogous peak in $D(\omega)$ for polymer systems is generally broader and shorter and varies little in height except at $p = 10^{-1}$, where it is also seen to blend into the bulk band [see Fig. 5(b) inset]. This indicates a consistently broader distribution of boundary-mode frequencies in polymer systems.

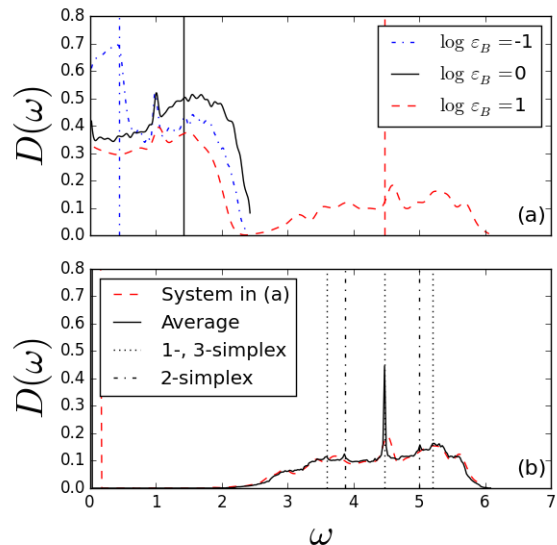


FIG. 6. $D(\omega)$ for $N = 2048$ polymer systems at $p = 10^{-4}$ and $0.1 \leq \varepsilon_B \leq 10$. (a) Three systems with $\varepsilon_0 = \varepsilon_W = 1$. Vertical lines indicate $\sqrt{2}\omega_B$. (b) $D(\omega)$ with $\varepsilon_0 = \varepsilon_W = 0, \varepsilon_B = 10$ for both the system in (a) and averaged over > 20 systems. Vertical lines indicate natural frequencies of regular simplices.

3. Backbone modes

Finally, we vary the stiffness of the backbone bonds in the polymer [Fig. 6(a)]. Backbone interactions lead to a broad band of vibrational states, approximately centered at $\sqrt{2}\omega_B \equiv \sqrt{2\varepsilon_B/m\sigma^2}$, as identified in Refs. [62, 63]. The broadness of this band may be contrasted with the narrower and more structured boundary-mode band in $D(\omega)$. Like the high- ε_W boundary band in Fig. 4, the high- ε_B backbone band's separation from the bulk band suggests a degree of independence in mode structure, and the density of states of the full system can be broken down into contributions from all three sources.

In Fig. 6(b), we replot $D(\omega)$ when $\varepsilon_B = 10$ for the system in Fig. 6(a) but set $\varepsilon_0 = \varepsilon_W = 0$ in our computation of $K_{ij}^{jj'}$. Bulk and boundary bands vanish into the δ -function peak of zero modes, but we observe almost no change in the backbone band, highlighting its independence from the bulk band. A universal feature of polymer vibrational spectra, the broad backbone band is a feature of real globular proteins [64, 65]. For better resolution of its features, we compute the average curve from > 20 systems. Several pronounced peaks appear in the backbone band, which are similar to the signatures of analytically-derived modes in collections of short chains of length $N_{\text{ch}} \leq 5$ in PBC [63]. The most pronounced peak is at $\omega = \sqrt{2}\omega_B$, which corresponds to the vibrational frequency of the 1-simplex (a single bond) as well as a normal mode of the general 3-simplex. There are also

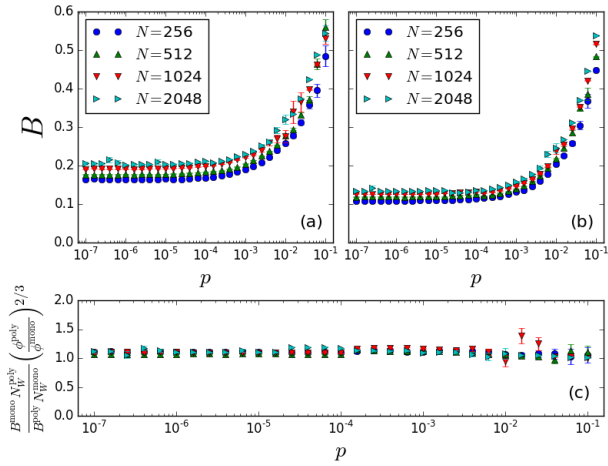


FIG. 7. Bulk modulus for (a) monomer and (b) polymer systems, (c) scaled B ratio.

small peaks at $\omega = \sqrt{2 \pm \frac{1}{2}\omega_B}$ and $\omega = \sqrt{2 \pm \sqrt{\frac{1}{2}\omega_B}}$, which correspond to vibrational frequencies of regular 2- and 3-simplices, respectively.

E. Bulk modulus

1. Effect of backbone connectivity

Plotting the bulk modulus $B \equiv \phi \partial p / \partial \phi$ of monomers and polymers over a range of $10^{-7} \leq p \leq 10^{-1}$ (Fig. 7), we find a constant, nonzero limit, $\lim_{p \rightarrow 0^+} B = B_0$, consistent with the power-law scaling relation $B \sim p^0$ [6, 7]. As pressure increases from zero, B remains within 1% of B_0 until $p \sim 10^{-4}$ while over this range N_S increases by orders of magnitude from $N_S = 1$ in the system sizes considered here (Fig. 1). B also varies with N , mostly due to variation of ϕ_J^N with system size (Fig. 2).

The bulk modulus is substantially ($\approx 40\%$) higher for monomers than for polymers. Variation in the prefactor ϕ in the definition of B accounts for only a small part of the difference; $\phi_J^{N,\text{poly}}$ is only $\approx 4\%$ lower than $\phi_J^{N,\text{mono}}$ [Fig. 2(c)]. Therefore, it must also be that $(\partial p / \partial \phi)^{N,\text{mono}} > (\partial p / \partial \phi)^{N,\text{poly}}$. Sec. IV A showed that the rigid subsystems are nearly equal in size between the two system types ($N^{\text{rigid,mono}} \approx N^{\text{rigid,poly}}$, $N_C^{\text{rigid,mono}} \approx N_C^{\text{rigid,poly}}$), so the difference in B must be due to configurational differences.

Recall that monomer packings have stronger layering and far more wall contacts than polymers (Sec. IV C). Only wall contacts couple the motion of the wall to the interior packing, and therefore we may expect B to rise with the wall contact density $N_W/A \sim N_W(\phi/N)^{2/3}$. In Fig. 7(c), we plot the ratio $\frac{B^{\text{mono}} N_W^{\text{poly}}}{B^{\text{poly}} N_W^{\text{mono}}} \left(\frac{\phi^{\text{poly}}}{\phi^{\text{mono}}} \right)^{2/3}$. We see that this ratio is approximately 1 for all system sizes and pressures, demonstrating that the difference in B is

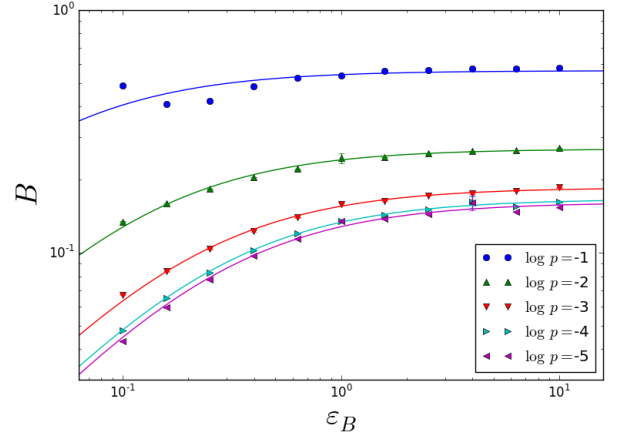


FIG. 8. Bulk modulus for $N = 2048$ polymer systems. Solid lines show curve-fitting to Eq. (15).

TABLE I. Curve-fitted parameters for Eq. (15).

$\log p$	B_∞	ϵ
-1	0.562 ± 0.005	0.039 ± 0.004
-2	0.2676 ± 0.0006	0.110 ± 0.002
-3	0.1854 ± 0.0004	0.194 ± 0.002
-4	0.1663 ± 0.0004	0.247 ± 0.003
-5	0.1612 ± 0.0008	0.260 ± 0.006

primarily due to N_W .

2. Effect of backbone stiffness

We also investigate the effect on B of the backbone stiffness by varying ϵ_B into both low-stiffness and high-stiffness regimes at pressures $10^{-5} \leq p \leq 10^{-1}$, plotted in Fig. 8. At low pressure, the bulk modulus vanishes if $\epsilon_B \rightarrow 0$, as the configuration without backbone bonds is under-coordinated for rigidity. The bulk modulus saturates to a constant as $\epsilon_B \rightarrow \infty$; backbone bonds become essentially inextensible compared to other contacts, yet the material can still deform around an infinitely stiff backbone. (In the equivalent case of decreasing ϵ_0 , recall that the units of ϵ_B and B are proportional to ϵ_0 , so that B decreases proportionally to ϵ_0 .)

To motivate a simple curve-fitting relation, consider that the material is isostatic at jamming, so the existence of the bulk modulus is dependent on every contact, similar to the simple situation of springs all in series. Given that B is measured by isotropically deforming the wall, we therefore consider a different system: a 1D chain of N_0^{eff} springs of stiffness $k_0 \equiv \epsilon_0/\sigma^2$ (these represent both wall and nonbonded-particle interactions since we have set $\epsilon_0 = \epsilon_W = 1$) and N_B^{eff} springs of stiffness $k_B \equiv \epsilon_B/\sigma^2$ (representing backbone interactions). The

chain's overall effective spring constant is

$$k_{\text{eff}} = \left(\frac{N_0^{\text{eff}}}{k_0} + \frac{N_B^{\text{eff}}}{k_B} \right)^{-1}, \quad (14)$$

which is proportional to the bulk modulus $B = \beta k_{\text{eff}}/\sigma$, where β is a dimensionless constant.

Rearranging Eq. (14) in terms of ε_B and $B_\infty = \lim_{\varepsilon_B \rightarrow \infty} B$ yields

$$B = B_\infty (1 + \varepsilon/\varepsilon_B)^{-1} \quad (15)$$

with $B_\infty = \beta k_0/\sigma N_0^{\text{eff}}$ and $\varepsilon = \sigma^2 k_0 N_B^{\text{eff}}/N_0^{\text{eff}}$. In natural units $\sigma = k_0 = 1$, the energy scale ε represents the ratio $N_B^{\text{eff}}/N_0^{\text{eff}}$.

We plot curve fits using Eq. (15) in Fig. 8, which agree well with data for $p \leq 10^{-2}$. The upward deviation in our data at $p = 10^{-1}$ for the lowest ε_B is a result of extreme compression and over-coordination as second-nearest-neighbor interactions occur, which the fitting form is not meant to capture. Pressure effects diminish in the low- p limit and curve-fitted values of ε and B_∞ are given in Table I.

V. DISCUSSION AND CONCLUSIONS

We have analyzed jammed configurations of a flexible bead-spring polymer in SC. Despite the presence of adhesive backbone bonds and spherical confining walls, the conditions at jamming largely carry over from the case of repulsive spheres in PBC. After accounting for the rigid-body motions within the spherical container, wall contacts, and under-constrained particles (rattlers/flippers), we see that jamming occurs exactly at isostaticity and coincides with the emergence of a single SSS. Jamming occurs at somewhat reduced density compared to monomers. Upon further compression, the number of SSSs scales as the square root of pressure, as for monomers in SC.

Confining walls and the polymer backbone influence the internal structure, density of states, and bulk modulus of the jammed material. The boundary causes layering in both local density and coordination, which are, unexpectedly, out of phase; qualitatively, curves for density and coordination are inverted in shape and phase-shifted $\approx \pi/2$. The boundary also introduces a narrow band of vibrational modes into the density of states with characteristic frequency scaling with the square root of the wall stiffness. At high wall stiffness, these modes are highly localized to the outermost two layers of sites. The independence of boundary modes from bulk modes extends to backbone modes; bands generated by high-stiffness backbone bonds are virtually unchanged after the removal of nonbonded and boundary potentials. Not only do these bands follow a universal pattern, but they also display peaks corresponding to regular low-dimensional

simplices, indicating the possibility of inferring aspects of the internal structure from the vibrational spectrum.

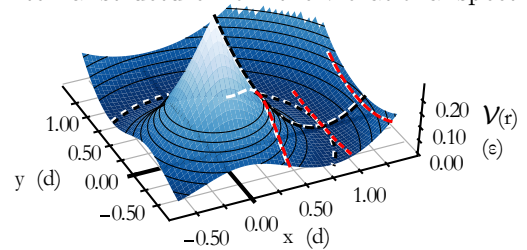


FIG. 9. Plot of the $z = 0$ potential energy surface $\mathcal{V}(r) = \varepsilon(1 - r/d)^2/2$, $r = \sqrt{x^2 + y^2 + z^2}$, to illustrate the curvature in the tangential direction of an extended or compressed harmonic interaction, and the higher-order stabilizing terms at zero pressure which are absent in the case of repulsive interactions.

The higher number of wall contacts in monomer packings raises the bulk modulus by $\approx 40\%$ compared to polymers. An explanation comes from a model of stiffnesses in series that scales with wall contact number. A similar conceptual model motivates a fitting relation that describes the dependence of the bulk modulus on the backbone stiffness.

Future analysis may investigate the material elasticity at higher pressure and with higher-curvature walls, where internal stresses and higher-order terms in the energy expansion are relevant. A fuller analysis may also investigate the spatial structure of SSSs and zero modes in SC or consider the effects of variable backbone stiffness, backbone-bending and dihedral stiffness, bond stresses, or attractive self-interactions.

ACKNOWLEDGMENTS

We are grateful for helpful discussions with Andrea Liu, Carl Goodrich, and Tom Lubensky. We thank the US DOE, Office of Basic Energy Sciences, Division of Materials Sciences and Engineering (Award DE-FG02-05ER46199) as well as the LRSM HPC cluster at the University of Pennsylvania for computational support.

Appendix: Explicit expansion of the interaction potentials

We explicitly calculate the lowest-order energy terms to analyze stability of a static configuration $\{\mathbf{r}_i^0\}$ after energy minimization, i.e., in force balance, with potential energy $\mathcal{E}_0 = \mathcal{E}(\{\mathbf{r}_i^0\})$. Let \mathbf{r}_i be the position of particle i and $\mathbf{u}_i = \mathbf{r}_i - \mathbf{r}_i^0$ be its displacement from its reference position. For small displacements, we can Taylor expand the energy,

$$\mathcal{E}(\{\mathbf{r}_i\}) = \mathcal{E}_0 + u_i^\mu \frac{\partial \mathcal{E}}{\partial r_i^\mu} \Big|_{\{\mathbf{r}_i^0\}} + \frac{u_i^\mu u_j^\nu}{2} \frac{\partial^2 \mathcal{E}}{\partial r_i^\mu \partial r_j^\nu} \Big|_{\{\mathbf{r}_i^0\}} + \cdots + \frac{\overbrace{u_i^\mu \cdots u_j^\nu}^n}{n!} \frac{\partial^n \mathcal{E}}{\partial r_i^\mu \cdots \partial r_j^\nu} \Big|_{\{\mathbf{r}_i^0\}} + \cdots, \quad (\text{A.1})$$

where repeated indices are summed over. The contribution proportional to displacement is necessarily zero since we expand about a minimum where the force on each particle vanishes ($-\partial \mathcal{E} / \partial r_i^\mu = 0$). The next derivatives in the expansion are readily calculated for our system, since \mathcal{E} is the sum of interaction energies [Eq. (1)]. Contributions at the n th order are n th-order derivatives of the interaction potentials, with $r_{ij}^0 = |\mathbf{r}_i^0 - \mathbf{r}_j^0|$.

All potentials in the simulation, where non-zero, have the form $\mathcal{V}(r) = \epsilon(1 - r/d)^2/2$. A displacement component parallel to the interaction direction $u_{\parallel} \equiv \mathbf{u} \cdot (\mathbf{r}_i^0 - \mathbf{r}_j^0)/r_{ij}^0$ corresponds to stiffness $\kappa \equiv \partial^2 \mathcal{V} / \partial u_{\parallel}^2 = \epsilon/d^2$. A component perpendicular $u_{\perp} \equiv |\mathbf{u} - u_{\parallel}(\mathbf{r}_i^0 - \mathbf{r}_j^0)/r_{ij}^0|$ also has finite stiffness, $\partial^2 \mathcal{V} / \partial u_{\perp}^2 = \kappa(1 - d/r)$, which is positive for wall-contacts and extended backbone bonds. The prefactors vanish in the unstressed, i.e., zero-energy limit, ($d = r$), so the energy costs of these motions appear only at $O(u_{\perp}^4)$ and have no linear response.

Therefore, at sufficiently low pressure, only relative motion in the direction normal to the contact contributes significantly to linear response, but higher-order terms

in the energy expansion can in principle affect jamming in some materials, e.g., they are seen to stabilize zero-frequency modes in packings of aspherical particles [66–68], thereby allowing a material to jam without all degrees of freedom in the rigid subsystem stabilized harmonically. At rest length, the nonzero contributions up to fourth order in the expansion come from the terms $\kappa u_{\parallel} u_{\perp}^2/6d$, $-\kappa u_{\parallel}^2 u_{\perp}^2/12d^2$, and $\kappa u_{\perp}^4/8d^2$. The curvature of the confining walls and the adhesive regime of the backbone bonds therefore contribute to stability at zero pressure at third order, and either positively or negatively to stability in fourth-order contributions depending on direction of the displacement in the pair potential. In principle, these terms may be able to stabilize zero modes in the packing or modes with instability that vanishes at zero pressure. Such modes would necessarily be decoupled from the compression deformation, so that the packing remains jammed with finite pressure. However, we do not observe zero-frequency modes other than rigid-body motions in these simulations after rattlers/flippers have been deleted, indicating that they tend not to appear in our sphere packings.

-
- [1] K. To, P.-Y. Lai, and H. K. Pak, *Phys. Rev. Lett.* **86**, 71 (2001).
 - [2] N. Keller, D. delToro, S. Grimes, P. J. Jardine, and D. E. Smith, *Phys. Rev. Lett.* **112**, 248101 (2014).
 - [3] Z. T. Berendsen, N. Keller, S. Grimes, P. J. Jardine, and D. E. Smith, *Proc. Nat. Acad. Sci. U.S.A.* **111**, 8345 (2014).
 - [4] N. Keller, S. Grimes, P. J. Jardine, and D. E. Smith, *Nat. Phys.* **12**, 757 (2016).
 - [5] C. S. O'Hern, S. A. Langer, A. J. Liu, and S. R. Nagel, *Phys. Rev. Lett.* **88**, 075507 (2002).
 - [6] C. S. O'Hern, L. E. Silbert, A. J. Liu, and S. R. Nagel, *Phys. Rev. E* **68**, 011306 (2003).
 - [7] A. J. Liu and S. R. Nagel, *Annu. Rev. Condens. Matter Phys.* **1**, 347 (2010).
 - [8] C. P. Goodrich, A. J. Liu, and S. R. Nagel, *Phys. Rev. Lett.* **109**, 095704 (2012).
 - [9] A. Kasahara and H. Nakanishi, *Phys. Rev. E* **70**, 051309 (2004).
 - [10] C. Song, P. Wang, and H. A. Makse, *Nature (London)* **453**, 629 (2008).
 - [11] L. E. Silbert, *Soft Matter* **6**, 2918 (2010).
 - [12] H. A. Vinutha and S. Sastry, *Nat. Phys.* **12**, 578 (2016).
 - [13] J. G. Berryman, *Phys. Rev. A* **27**, 1053 (1983).
 - [14] S. Torquato, T. M. Truskett, and P. G. Debenedetti, *Phys. Rev. Lett.* **84**, 2064 (2000).
 - [15] G. D. Scott, *Nature (London)* **188**, 908 (1960).
 - [16] J. D. Bernal and J. Mason, *Nature (London)* **188**, 910 (1960).
 - [17] G. D. Scott and D. M. Kilgour, *J. Phys. D* **2**, 863 (1969).
 - [18] A. S. Clarke and J. D. Wiley, *Phys. Rev. B* **35**, 7350 (1987).
 - [19] N. C. Karayiannis and M. Laso, *Macromolecules* **41**, 1537 (2008).
 - [20] N. C. Karayiannis and M. Laso, *Phys. Rev. Lett.* **100**, 050602 (2008).
 - [21] K. Foteinopoulou, N. C. Karayiannis, M. Laso, M. Kröger, and M. L. Mansfield, *Phys. Rev. Lett.* **101**, 265702 (2008).
 - [22] N. C. Karayiannis, K. Foteinopoulou, and M. Laso, *Phys. Rev. E* **80**, 011307 (2009).
 - [23] N. C. Karayiannis, K. Foteinopoulou, and M. Laso, *Philos. Mag.* **93**, 4108 (2013).
 - [24] N. C. Karayiannis, K. Foteinopoulou, and M. Laso, *J. Chem. Phys.* **130**, 164908 (2009).
 - [25] N. C. Karayiannis, K. Foteinopoulou, and M. Laso, *Phys. Rev. Lett.* **103**, 045703 (2009).
 - [26] N. C. Karayiannis, K. Foteinopoulou, C. F. Abrams, and M. Laso, *Soft Matter* **6**, 2095 (2010).
 - [27] R. S. Hoy and N. C. Karayiannis, *Phys. Rev. E* **88**, 012601 (2013).
 - [28] R. S. Hoy, *Phys. Rev. Lett.* **118**, 068002 (2017).
 - [29] R. P. Zou and A. B. Yu, *Chem. Eng. Sci.* **50**, 1504 (1995).
 - [30] G. T. Seidler, G. Martinez, L. H. Seeley, K. H. Kim, E. A.

- Behne, S. Zaranek, B. D. Chapman, S. M. Heald, and D. L. Brewster, *Phys. Rev. E* **62**, 8175 (2000).
- [31] S. Ghosh, D. Wijnperl, F. Mugelea, and M. H. G. Duits, *Soft Matter* **12**, 1621 (2016).
- [32] K. S. Liu, M. H. Kalos, and G. V. Chester, *Phys. Rev. A* **10**, 303 (1974).
- [33] J. Mittal, T. M. Truskett, J. R. Errington, and G. Hummer, *Phys. Rev. Lett.* **100**, 145901 (2008).
- [34] A. K. Macpherson, Y. P. Carignan, and T. Vladimiroff, *J. Chem. Phys.* **87**, 1768 (1987).
- [35] J. W. Landry, G. S. Grest, L. E. Silbert, and S. J. Plimpton, *Phys. Rev. E* **67**, 041303 (2003).
- [36] K. W. Desmond and E. R. Weeks, *Phys. Rev. E* **80**, 051305 (2009).
- [37] J.-F. Camenen, Y. Descantes, and P. Richard, *AIP Conf. Proc.* **1542**, 321 (2013).
- [38] L. C. Verman and S. Banerjee, *Nature (London)* **157**, 584 (1946).
- [39] R. L. Brown and P. G. W. Hawksley, *Nature (London)* **157**, 585 (1946).
- [40] R. Dickman and C. K. Hall, *J. Chem. Phys.* **89**, 3168 (1988).
- [41] I. Bitsanis and G. Hadziioannou, *J. Chem. Phys.* **92**, 3827 (1998).
- [42] L.-N. Zou, X. Cheng, M. L. Rivers, H. M. Jaeger, and S. R. Nagel, *Science* **326**, 408 (2009).
- [43] L. M. Lopatina, C. J. OlsonReichhardt, and C. Reichhardt, *Phys. Rev. E* **84**, 011303 (2011).
- [44] J.-M. Y. Carrillo and B. G. Sumpter, *J. Chem. Phys.* **141**, 074904 (2014).
- [45] A. Nikoubashman, D. A. Vega, K. Binder, and A. Milchev, *Phys. Rev. Lett.* **118**, 217803 (2017).
- [46] J. Kindt, S. Tzlil, A. Ben-Shaul, and W. M. Gelbart, *Proc. Nat. Acad. Sci. U.S.A.* **98**, 13671 (2001).
- [47] J. Arsuaga, R. K.-Z. Tan, M. Vazquez, D. W. Sumners, and S. C. Harvey, *Biophys. Chem.* **101–102**, 475 (2002).
- [48] J. C. LaMarque, T. L. Le, and S. C. Harvey, *Biopolymers* **73**, 348 (2004).
- [49] I. Ali, D. Marenduzzo, and J. M. Yeomans, *J. Chem. Phys.* **121**, 8635 (2004).
- [50] A. J. Spakowitz and Z.-G. Wang, *Biophys. J.* **88**, 3912 (2005).
- [51] D. Marenduzzo, E. Orlandini, A. Stasiak, D. W. Summers, L. Tubiana, and C. Micheletti, *Proc. Nat. Acad. Sci. U.S.A.* **106**, 22269 (2009).
- [52] D. Marenduzzo, C. Micheletti, and E. Orlandini, *J. Phys.: Condens. Matter* **22**, 283102 (2010).
- [53] S. Plimpton, *J. Comp. Phys.* **117**, 1 (1995).
- [54] E. Bitzek, P. Koskinen, F. Gähler, M. Moseler, and P. Gumbsch, *Phys. Rev. Lett.* **97**, 170201 (2006).
- [55] T. C. Lubensky, C. L. Kane, X. Mao, A. Souslov, and K. Sun, *Rep. Prog. Phys.* **78**, 109501 (2015).
- [56] J. C. Maxwell, *Philos. Mag.* **27**, 294 (1864).
- [57] C. Ness, V. V. Palyulin, R. Milkus, R. Elder, T. Sirk, and A. Zaccane, *Phys. Rev. E* **96**, 030501 (2017).
- [58] C. O. Plaza-Rivera, H. T. Nguyen, and R. S. Hoy, *Soft Matter* **13**, 7948 (2017).
- [59] A. S. Clarke and H. Jónsson, *Phys. Rev. E* **47**, 3975 (1993).
- [60] A. V. Anikeenko and N. N. Medvedev, *Phys. Rev. Lett.* **98**, 235504 (2007).
- [61] N. W. Ashcroft and N. D. Mermin, *Solid State Physics*, 1st ed. (Cengage Learning, New York, 1976).
- [62] T. S. Jain and J. J. de Pablo, *J. Chem. Phys.* **120**, 9371 (2004).
- [63] R. Milkus, C. Ness, V. V. Palyulin, J. Weber, A. Lapkin, and A. Zaccane, *Macromolecules* **51**, 1559 (2018).
- [64] D. ben Avraham, *Phys. Rev. B* **47**, 14559 (1993).
- [65] H. Na, G. Song, and D. ben Avraham, *Phys. Biol.* **13**, 016008 (2016).
- [66] A. Donev, R. Connelly, F. H. Stillinger, and S. Torquato, *Phys. Rev. E* **75**, 051304 (2007).
- [67] M. Mailman, C. F. Schreck, C. S. O'Hern, and B. Chakraborty, *Phys. Rev. Lett.* **102**, 255501 (2009).
- [68] K. VanderWerf, W. Jin, M. D. Shattuck, and C. S. O'Hern, *Phys. Rev. E* **97**, 012909 (2018).